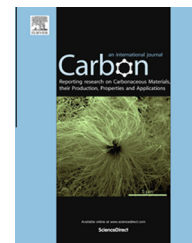


Available at www.sciencedirect.com

ScienceDirect

journal homepage: www.elsevier.com/locate/carbon

Shock formation and rate effects in impacted carbon nanotube foams



Ramathasan Thevamaran ^{a,b}, Eric R. Meshot ^c, Chiara Daraio ^{a,b,*}

^a Division of Engineering and Applied Sciences, California Institute of Technology, Pasadena, CA 91125, USA

^b Dept. of Mechanical and Process Engineering, Swiss Federal Institute of Technology Zurich (ETH Zurich), Zurich 8092, Switzerland

^c Physical and Life Sciences Directorate, Lawrence Livermore National Laboratory, Livermore, CA 94551, USA

ARTICLE INFO

Article history:

Received 21 August 2014

Accepted 1 December 2014

Available online 5 December 2014

ABSTRACT

We investigate rate-effects in the dynamic response of vertically aligned carbon nanotube (VACNT) foams excited by impacts at controlled velocities. They exhibit a complex rate-dependent loading-unloading response at low impact velocities and they support shock formation beyond a critical velocity. The measured critical velocities are ~ 10 times lower than in other foams of similar densities—a desirable characteristic in impact protective applications. *In-situ* high-speed microscopy reveals strain localization and progressive buckling at low velocities and a crush-front propagation during shock compression. We correlate these responses to quantitative measurements of the density gradient and fiber morphology, obtained with spatially resolved X-ray scattering and mass attenuation.

© 2014 Elsevier Ltd. All rights reserved.

1. Introduction

Carbon nanotube (CNT) arrays can be fabricated to different scales: from microscopic, regular patterns of individual tubes for electronic and sound applications [1–3], to bulk and entangled macrostructures, for mechanical and textile applications [4,5]. For example, long fibers and yarns have been produced for bulletproof tough textiles and conductive electronic textiles [4,5]. Sheets of CNTs have been fabricated for transparent highly elastomeric electrodes [6] and underwater thermoacoustic projectors [2]. Thin film bucky papers made of randomly oriented individual carbon nanotubes have also been studied for energy storage and chemical catalysis [7,8]. In bulk, vertically aligned carbon nanotube (VACNT) arrays [3,9,10] and non-aligned inter-connected sponge like structures [11] have been investigated for energy dissipative cushioning and packaging, super-capacitor, catalytic electrodes, super hydrophobic surfaces and tissue engineering

scaffolds. Freestanding VACNT arrays exhibit intriguing mechanical responses that, for example, make them the most efficient low-density, energy absorbing material known [10,12,13]. These properties arise from their intrinsic complex deformation behavior, which opens up fundamental areas of investigation in mechanics, and serves as a controlled model to understand the response of hierarchical materials with a fibrous morphology.

Macroscale VACNT foams have constituents at different length scales, forming a hierarchical structure: entangled individual multi-walled carbon nanotubes (MWCNTs) at the nanoscale, a seemingly disordered forest at the microscale, and vertically aligned bundles at the mesoscale. The properties and morphologies of the constituent structures are highly dependent on the synthesis conditions [14] and they play an important role in determining the mechanical response of the bulk foams. Subjected to quasistatic compressive loading, freestanding VACNT foams exhibit super-compressibility and

* Corresponding author at: Dept. of Mechanical and Process Engineering, Swiss Federal Institute of Technology Zurich (ETH Zurich), Zurich 8092, Switzerland.

E-mail address: daraio@ethz.ch (C. Daraio).

<http://dx.doi.org/10.1016/j.carbon.2014.12.006>

0008-6223/© 2014 Elsevier Ltd. All rights reserved.

have the ability to recover from large strains of up to 80% upon unloading [10,15]. Their deformation response is highly localized and in compression these foams support the formation of sequential buckles, originating from anisotropic, graded functional properties. They also show high fatigue resistance, surviving tests of up to a million compressive cycles at moderate strains [16]. The fundamental characteristics of nucleation and propagation of sequential periodic buckling, observed first at the macroscale [10], was confirmed in micro-pillars using *in-situ* indentation experiments inside a scanning electron microscope (SEM) [17,18].

Studies of rate effects on the mechanical response of bulk CNT foams have focused on the quasistatic regime or on the linear dynamic regime. Uniaxial compression cycles performed at up to 80% strain in the quasistatic regime (10^{-4} – 10^{-1} s $^{-1}$) have shown a rate-independent mechanical response [19]. In contrast, faster, but still quasi-static, strain rates (up to 0.04 s $^{-1}$ [13] and up to 1 s $^{-1}$ [20]) suggested rate effects on recovery [13] and unloading modulus [13,20]. In both reports the recovery and elastic unloading modulus were shown to increase with increasing deformation rates. In the linear dynamic regime, uniaxial nano-dynamic mechanical analysis (nano-DMA) at small amplitudes (3–50 nm; 0.7% strain) showed no dependence of the CNT foam's response on the driving frequency [21]. However, they reported dependence of the storage and loss moduli on the driving amplitude and the variation of the foam's microstructure. Large amplitude DMA performed in torsion-mode (shear) also exhibited temperature and frequency invariant viscoelasticity between 0.1–100 Hz and –196–1000 °C temperatures [22]. Coarse-grained molecular dynamics simulations and triboelastic constitutive models supported these experimental observations [23]. It should be noted that the fundamental deformation mechanisms in uniaxial compression involving bending, buckling and microstructural rearrangements [10,21] are significantly different from the zipping, unzipping and bundling observed in torsion-mode (shear) DMA [22,23].

Drop-ball tests performed on VACNT forests demonstrated their ability to mitigate impacts [24,25] at high-rate deformations. However, the deformation behavior and the fundamental dissipative mechanisms at high rates and for finite deformations are not thoroughly understood due to the difficulties in obtaining dynamic displacement measurements with microscale resolutions.

In this article, we report a detailed experimental study on the response of CNT foams subjected to controlled, high-rate impacts, reaching up to 95% strain, using time-resolved dynamic displacement and force measurements. This study provides a thorough understanding of fundamental dynamic deformation mechanisms in the micro- and macro-scales and identifies different dynamic regimes—localized buckling and shock formation—supported by the VACNT foams.

2. Experimental

2.1. Sample synthesis

The VACNT foams were synthesized using a floating catalyst thermal chemical vapor deposition (tCVD) process with

feedstock consisting of ferrocene (catalyst precursor) and toluene (carbon source) mixed at 0.02 g ml $^{-1}$. The feedstock solution was injected at 0.75 ml min $^{-1}$ into the carrier gas, typically consisting of hydrogen balanced with argon, delivered at a total rate of 800 sccm. Oxidized silicon substrates were placed inside a 15 cm hot zone of a quartz furnace tube for bottom-up VACNT foam growth. The furnace tube was maintained at 827 °C and atmospheric pressure throughout the synthesis. The resultant VACNT foams had thicknesses in the order of a millimeter. Hydrogen concentration in the carrier gas was varied between 30% and 5% to produce VACNT foams with tailored microstructures and different bulk densities, varying from 0.1 to 0.3 g cm $^{-3}$. These different microstructures were shown to present mechanical properties varying over a broad range in the quasistatic regime [26]. The synthesized specimens were extracted from the substrate using a custom-made core drill and prepared for dynamic testing.

2.2. Structural characterization

We performed synchrotron X-ray scattering and mass attenuation measurements to nondestructively quantify the density and alignment within the VACNT foams. We used an incident photon energy of 10 keV with a beam height of less than 300 μ m at the sample in order to spatially map structural characteristics along the vertical height of our millimeter-thick foams. Monitoring the drop in X-ray intensity across the sample enabled determination of mass density using the Beer-Lambert law [27], and CNT alignment was quantified from the anisotropy of wide-angle X-ray scattering (WAXS) patterns using the Herman's orientation factor, f [28,29]. Here, f equals 1 for perfectly aligned CNTs and 0 for random order (no alignment). Details on the analysis and results can be found in the [Supplementary information \(S1 and S2\)](#). Briefly, our results show a gradient in VACNT mass density for the synthesis conditions used in our study, with a monotonic decay towards the bottom (corresponding to the end of growth) (Fig. S2(a) and (b)). This agrees with previous results for growth from substrate bound thin-film catalysts [30], but to our knowledge this is the first direct confirmation of density decay in floating catalyst growth of VACNTs. Our CNTs are highly aligned with $f=0.6$ on average, and we determined that alignment is directly correlated with density (Fig. S2(d)), which has a strong influence on the mechanical performance. With decreasing hydrogen concentrations, the density of the VACNT foam increases, and the CNTs exhibit higher vertical alignment. The following results and discussions draw important quantitative relationships between the structural characteristics of the VACNT foams and their advanced mechanical properties.

2.3. Dynamic characterization

We developed an experimental setup to deliver controlled and repeatable flat-plunge striker impacts on CNT foams, ranging impact velocities from 0.5 to 10 ms $^{-1}$ [31]. The dynamic forces are measured using a dynamic force sensor mounted at a stationary wall target. The setup is equipped with a geometric

moiré interferometer for measuring dynamic displacement history and a high-speed microscopic camera for *in-situ* identification of the microscale localized dynamic deformation. The displacements are measured with a $6.25\ \mu\text{m}$ spatial resolution on the moiré transducer. We operate the high-speed microscopic camera for *in-situ* visualization at a frame rate of $\sim 150,000$ fps and a resolution of 128×256 pixels, focused on a physical window of $\sim 1.8\ \text{mm} \times 3.5\ \text{mm}$. Details of the dynamic testing methods can be found in [31] and the calculations of all mechanical parameters are described in the [Supplementary information \(S3\)](#).

3. Results and discussions

The effects of increasing loading rates on a VACNT foam are reported in Fig. 1. We show a hysteretic response and the presence of preconditioning effects, similar to what was reported in the quasistatic regime [10,19]. The presence of hysteresis accounts for the energy dissipated during impact loading and unloading. The preconditioning effects are evident when the same specimen is impacted with increasing loading rates. During the first impact, the sample follows a large hysteretic path, characteristic of a pristine (as-grown) sample. As the sample is impacted again with a higher impact velocity, the loading path follows initially a preconditioned response, and then changes to that of the pristine specimen, when the strain exceeds the maximum strain reached in the

prior impact (Fig. 1(a)). This behavior confirms the strain localization found in quasistatic tests as well [19]. In addition, it demonstrates that the samples' loading responses are rate-independent, over a broad range of impact velocities from 1 to $6\ \text{ms}^{-1}$ (nominal strain rates: 1000 – $6000\ \text{s}^{-1}$). This rate-independent loading response is further verified by comparing the quasistatic compression cycles performed at $0.01\ \text{s}^{-1}$ strain rate to the dynamic stress–strain cycles (Fig. 1(a)). To verify that the rate-independent loading response is not a function of a sample's loading history, we tested several pristine specimens at different impact velocities. A corresponding set of characteristic stress–strain curves is shown on Fig. 1(b).

The unloading response shows the presence of rate effects. This is verified by plotting the dynamic unloading modulus (E_{dyn}), normalized by the quasistatic unloading modulus (E_s), at maximum strain, against the nominal strain rate measured at the moment of impact (inset of Fig. 1(b)). The normalized unloading modulus increases with the strain rate, suggesting the presence of rate effects during the recovery phase of the dynamic deformation. During the formation of collective buckles of CNT-bundles in loading phase, new van der Waals interactions would occur between the buckle folds. The snap-back recovery of the collective buckles primarily depends on overcoming the energy required to break those van der Waals interactions. The required energy is derived from the energy that is stored elastically during the loading phase. Our observations imply that these recovery mechanisms of collective buckles are rate-sensitive.

To explore the effects of foam's microstructure on the bulk dynamic response, we performed similar experiments on VACNT foams with varying bulk densities (0.1 – $0.3\ \text{g cm}^{-3}$). Characteristic stress–strain responses obtained at similar impact velocities for a low-density foam and a high-density foam are shown in Fig. 2. The low-density foams exhibit a response that is more similar to the typical foam materials [32], with a pronounced initial linear regime that is followed by a prolonged plateau regime at moderate stress levels (Fig. 2(a)). The high-density foam, however, does not exhibit any distinct linear regime and shows a highly nonlinear rise of stress in strain (Fig. 2(b)) instead of a prolonged plateau regime. We correlate the presence of pronounced linear regime in the low-density foams to their less-aligned microstructure—characterized by the Herman's orientation factor of 0.54 (Fig. S2(d))—that closely resembles that of the open-cell foams. Such effects of microstructure have also been observed previously in quasistatic compression, and attributed primarily to the differences in diameter distribution of the CNT population among samples synthesized with different hydrogen concentrations [26]. The increase in hydrogen concentration has been shown to result in narrower diameter distribution [26], which may affect the stress at which the collective buckles form, and their progression. In addition to these characteristics of the stress–strain responses, the foam's microstructure significantly affects the bulk mechanical response. The VACNT foams become more compliant with decreasing bulk density and results in large deformations at low stress levels (Fig. S4). In contrast, high-density foams deform less and reach higher peak stresses during impact (Fig. S4).

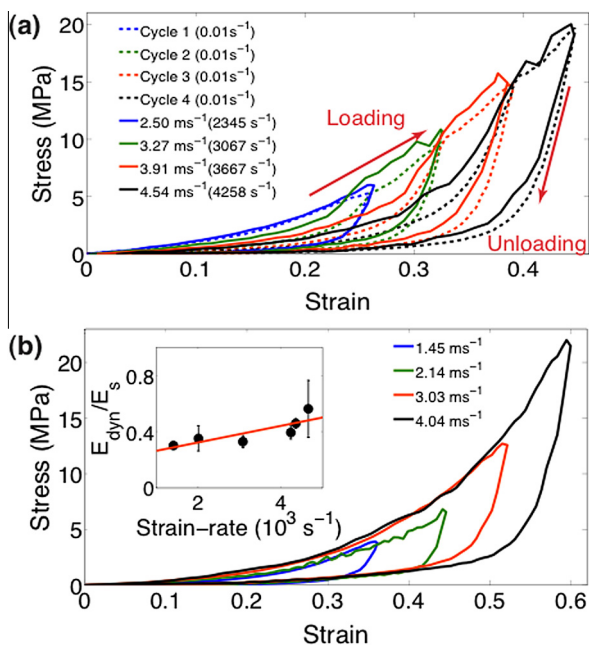


Fig. 1 – (a) Dynamic response of a VACNT foam subjected to several impacts at increasing controlled velocities (solid lines) compared to a similar VACNT foam subjected to quasistatic compressive cyclic loading (dashed lines). (b) Dynamic response of different pristine VACNT foams of similar densities, at increasing impact velocities. The inset shows the dynamic unloading modulus normalized by the quasistatic unloading modulus at given maximum strains reached during impact. (A color version of this figure can be viewed online.)

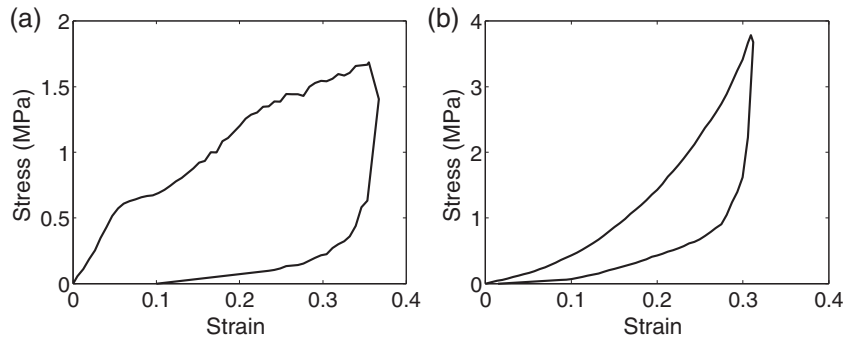


Fig. 2 – Effect of the microstructure on the bulk dynamic stress–strain response of the VACNT foams. The characteristic stress–strain responses correspond to VACNT foams synthesized with (a) 30% hydrogen concentration (bulk density, 0.15 g cm^{-3} ; impact velocity, 1.35 ms^{-1}) and (b) 5% hydrogen concentration (bulk density, 0.26 g cm^{-3} ; impact velocity, 1.42 ms^{-1}).

A summary of the mechanical properties for various samples tested at a broad range of impact velocities can be found in Fig. 3. The peak stress increases with impact velocity (Fig. 3(a)) and maximum strain (Fig. 3(b)). It should be noted that the increase in the peak stress with impact velocity is not due to rate effects, but a natural consequence of the increasing maximum strain reached upon impact. Due to the gradient in density along the height of the foam as well as the densification that occurs during loading, the peak stress increases with increasing maximum strain. The unloading modulus also increases with the increasing maxi-

um strain reached (Fig. 3(c)). The relation of the unloading modulus and the energy dissipation with increasing impact velocities is shown in Fig. S5. Similar to peak stress, the increase of unloading modulus and energy dissipation with the increasing impact velocities (therefore, with increasing maximum strain) is attributed to the density gradient that is present along the height of the foam, and the densification that occurs during loading. For a given impact velocity, VACNT foams with higher bulk densities exhibit stiffer responses characterized by higher peak stresses and unloading moduli (Figs. 3 and S5).

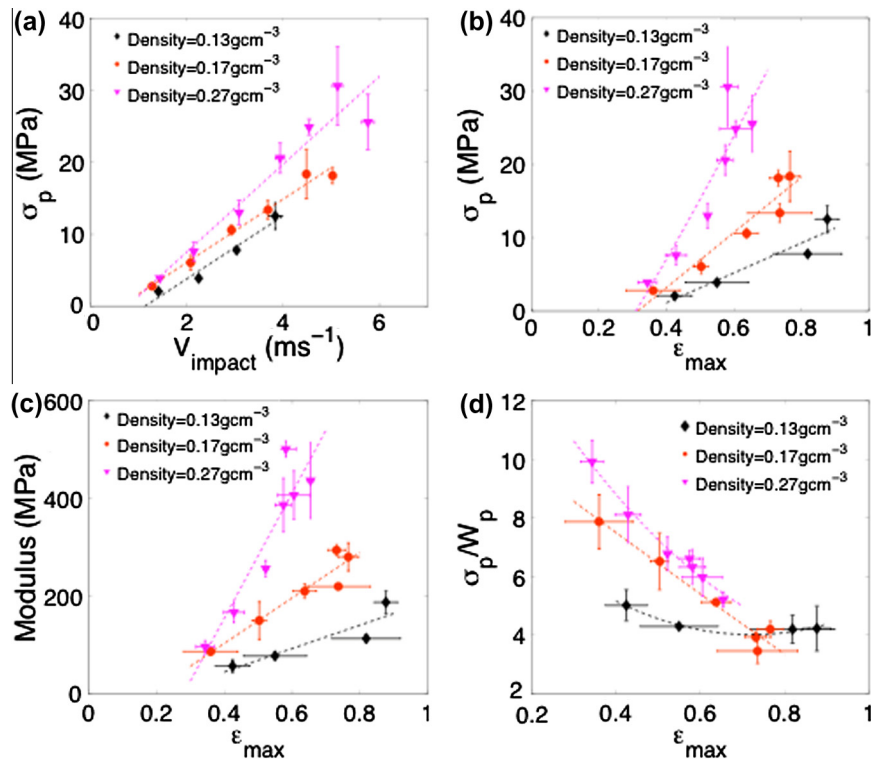


Fig. 3 – Dynamic response of VACNT foams with average bulk densities of 0.13 ± 0.02 , 0.17 ± 0.02 and $0.27 \pm 0.02 \text{ g cm}^{-3}$ (the horizontal and vertical error bars represent the standard deviation of the three samples tested in each case). (a) Variation of peak stress with the striker impact velocity; (b) variation of peak stress with the maximum strain reached during impact; (c) variation of the unloading modulus with the maximum strain reached during impact; (d) variation of the dynamic cushion factor—peak stress divided by energy absorbed up to peak stress—with the maximum strain reached during impact. (A color version of this figure can be viewed online.)

We use the dynamic cushion factor, given by the peak stress divided by the energy absorbed up to the peak stress (σ_p/W_p), to characterize the damping efficiency of the VACNT foams. In general, a low cushion factor is beneficial for impact mitigation and energy dissipative applications. Both the increase in the energy absorption and the decrease in the peak stress contribute to reducing the cushion factor. To characterize the quasistatic response of conventional foam materials, the static cushion factor is plotted against the plateau stress [32]. This was also reported for the quasistatic response of disordered carbon nanotubes [33]. In dynamics, we plot (Fig. 3(d)) the cushion factor against the maximum strain reached to combine all the critical parameters of the impact response: the peak stress, maximum strain and the energy absorption. A conventional plot of the dynamic cushion factor with peak stress is given on Fig. S6.

VACNT foams with lower densities perform well in mitigating impact force and absorbing energy for a given maximum strain, at low velocity impacts ($<3\text{ ms}^{-1}$; striker mass = 7.1 g) (Fig. 3(d)). When subjected to high velocity impacts, however, they rapidly reach the densification strain, posing a performance limit. VACNT foams with higher densities exhibit higher moduli and deform less and are capable of absorbing high velocity impacts. In the quasistatic regime, the energy dissipated by these VACNT foams was found to be more than 200 times higher than the energy dissipated by commercial foams of similar densities [12]. We qualitatively demonstrate the protective properties of CNT foams compared to those of a commercial polymeric foam with similar density ($\sim 0.2\text{ g cm}^{-3}$) and thickness ($\sim 1\text{ mm}$), by dropping two eggs from the same height ($\sim 0.5\text{ m}$) with each foam installed on their surfaces to absorb the impact (Supplementary Video 1). In this educational video, we show that the egg protected by VACNT foams remains intact after the impact that reaches velocities of up to $\sim 3\text{ ms}^{-1}$, whereas the commercial polymeric foam installed egg cracks during impact.

To compare the performance of the VACNT foams with that of other materials in the literature [34–38], we plot the elastic modulus as a function of the bulk density. For these plots, the unloading modulus of the VACNT foams was chosen over the loading modulus as the characteristic stiffness, since it represents the elastic recoiling of the VACNT foams after the impact (Fig. 4). For the CNT foams, we show a range of dynamic unloading moduli arising from different maximum deformations reached at different impact velocities. For simplicity, they are grouped into three different ranges of maximum strains: 0.35–0.49 (with avg. 0.40), 0.50–0.69 (with avg. 0.60) and 0.70–0.88 (with avg. 0.75). The results follow a linear correlation in the double-logarithmic plot, implying a power-law relationship between the modulus and the density similar to the one found in conventional foam materials [32]. VACNT foams always present the highest elastic moduli at a given bulk density when compared to other foam materials.

The *in-situ* visualization using high-speed microscopic imaging provided insights into the fundamental mechanisms of deformations. When the striker impacted the sample, due to the density gradient along the thickness of the VACNT foams, buckling instabilities nucleated in the low-density region of the samples and propagated sequentially towards the high-density region. The initial buckle formation always

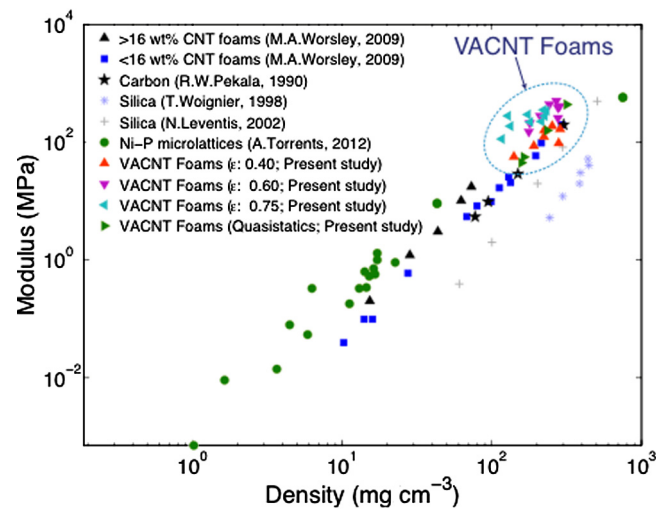


Fig. 4 – Dynamic and quasistatic unloading moduli of VACNT foams as a function of the average bulk density, in comparison with the moduli of similar foam-like materials found in literature [34–38]. (A color version of this figure can be viewed online.)

occurred at the low-density region independently of the impacted side of the sample, implying the strong influence of the intrinsic density gradient. The characteristic intrinsic density gradient measured by synchrotron X-ray scattering and mass attenuation in our samples is shown in the inset of Fig. 5(a) (see also Fig. S2(a) and (b)). Due to the nonlinear density gradient observed for VACNT foams, when impacted, we observed an increase in buckle wavelength along the height (Supplementary Video 2). The samples recovered the deformation upon unloading. A few snapshots of the dynamic deformation are provided in Fig. 5(a), along with the corresponding dynamic stress–strain diagram for an impact velocity of 1.75 ms^{-1} . From Supplementary Video 2 it can be seen that the VACNT foams exhibit high resilience to impact with 100% instantaneous recovery. On average, the samples with different densities recovered $83 \pm 10\%$ of the dynamic deformation. The characterization of the samples using scanning electron microscopy (SEM) after high velocity impacts ($\sim 6\text{ ms}^{-1}$), showed traces of permanent collective buckling (Fig. 5(b)). Transmission electron microscopic (TEM) imaging of these specimens revealed individual MWCNTs with wrinkled outer walls (Fig. 5(c)). Similar permanent defects of wrinkled outer walls on the compression side of the tube were also reported in earlier dynamic tests of CNT foams [25] and highly bent individual MWCNTs [39].

The reported rate-independent dynamic loading behavior transitions into shock formation at a critical impact velocity, characteristic of bulk densities (Fig. 6(a–d)). We have observed this behavior in VACNT foams with a $0.13 \pm 0.02\text{ g cm}^{-3}$ average bulk density, at impact velocities of $\sim 5\text{ ms}^{-1}$, and for denser VACNT foams ($\sim 0.2\text{ g cm}^{-3}$), at $\sim 6.5\text{ ms}^{-1}$ (Fig. S7). These critical velocities are surprisingly low (more than 10 times lower) compared to the critical shock formation velocities observed in metallic open-cell foams with comparable bulk densities and elastic moduli [40,41] (Aluminum open-cell

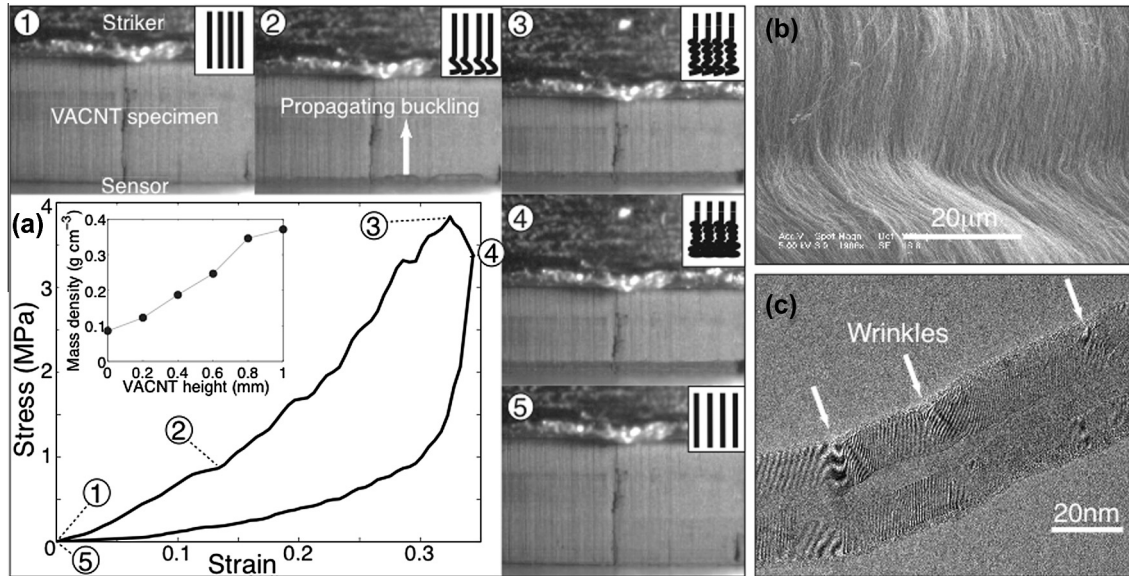


Fig. 5 – (a) Deformation micrographs obtained from high-speed microscopic imaging, for a VACNT foam impacted at 1.75 ms^{-1} (Supplementary Video 2); inset shows the intrinsic density variation along the height of a VACNT foam with mean density 0.23 g cm^{-3} . (b) SEM image of the collective permanent buckles in a VACNT foam impacted at $\sim 5 \text{ ms}^{-1}$ (the scale bar is $20 \mu\text{m}$). (c) TEM image of an individual multiwalled carbon nanotube exhibiting wrinkles on walls caused by buckling (the scale bar is 20 nm). (A color version of this figure can be viewed online.)

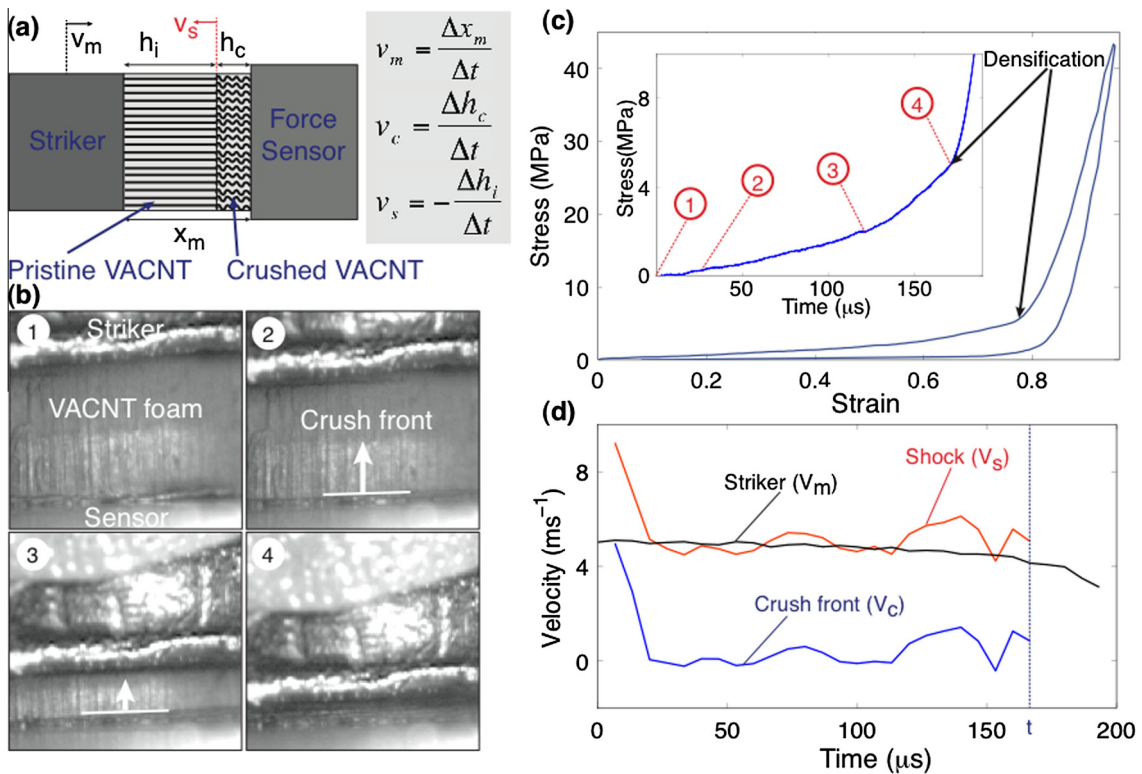


Fig. 6 – (a) Schematic illustration of shock formation in VACNT foams identifying the shock parameters. (b) Snapshots from the high-speed camera imaging sequence showing the formation and propagation of the shock wave. (c) Stress–strain diagram showing the loading–unloading response during impact. Inset shows the loading phase up to densification; the circles 1–4 indicate instances corresponding to the high-speed camera images. (d) Evolution of the shock, crush-front and striker velocities during the loading phase. Time t indicates the instance when the shock wave reaches the specimen–striker interface, beyond which the crushed VACNT foam is compressed through densification. (A color version of this figure can be viewed online.)

foams compared here have average bulk density $\sim 0.22 \text{ g cm}^{-3}$; average longitudinal modulus $\sim 593 \text{ MPa}$ and transverse modulus $\sim 338 \text{ MPa}$). When the samples were impacted at velocities higher than these critical velocities, we observed a distinct crush front propagating from the low-density region (Supplementary Video 3). During the loading phase, the stress increased almost linearly with strain at moderate stress levels. Beyond the densification strain (~ 0.8), the stress increased rapidly to very high values. During the unloading phase, the stress dropped rapidly and the strain presented a significant recovery ($86 \pm 8\%$). A characteristic stress–strain response and the corresponding loading stress–time history for a shocked specimen (with density 0.12 g cm^{-3} , impacted at 5.02 ms^{-1}) are shown in Fig. 6(c). A few snapshots from the high-speed image sequence identifying the propagation of the crush front are shown in Fig. 6(b). In this case, the stress–strain response of the samples changes dramatically, presenting a much narrower hysteresis, a sharper transition to the densification regime and no characteristic saw-tooth pattern identifying the buckles formation in quasi-static compression. The crush front in Supplementary Video 3 proceeds continuously compressing the samples without allowing time for the sequential buckle formation, seen in the low velocity Supplementary Video 2. A set of stress–strain diagrams comparing the dynamic responses at subcritical impact velocity, and during shock compression are given in Supplementary Fig. S7, for low-density foams (Fig. S7(a)) and high-density foams (Fig. S7(b)). The above described dramatic changes in the hysteresis, and the differences in deformation modes characterized by the presence of or lack thereof local instabilities can be seen in Fig. S7.

The parameters used to calculate the crush front speed and the shock front speed are shown in the schematic diagram in Fig. 6(a) [40]. The evolution of the striker velocity (V_m), the crush front velocity (V_c) and the shock velocity (V_s) during the shock compression is shown in Fig. 5(d). The time $t = 166 \mu\text{s}$ corresponds to the instance the shock reaches the striker–VACNT foam interface. During this time, the striker decelerates from 5.02 ms^{-1} to 4.13 ms^{-1} , beyond which it rapidly decelerates to zero as the material is compressed beyond its densification strain. The shock velocity reduces from $\sim 9 \text{ ms}^{-1}$ to $\sim 5 \text{ ms}^{-1}$ and remains nearly steady until time $t = 166 \mu\text{s}$. The crush front propagates initially at the impact velocity of the striker, and then rapidly reduces to $\sim 0.5 \text{ ms}^{-1}$ and remains steady as more material piles up behind the shock. All velocities were calculated by processing the high-speed image sequence using commercial image correlation software (*Image systems, TEMA*). We attribute the presence of oscillations on the shock and the crush front velocities to the discrete time steps of the high-speed image sequence.

The experimental evidence of shock formation in VACNT foams provides critical insights into the influence of graded, fibrous microstructure on the formation and propagation of shock waves. For example, the presence of a density gradient in VACNT foams confines the shock formation in the low-density region of the sample and the shock front progresses towards increasing density. This is reflected also in the stress–time history profile: homogeneous foams present a sharp initial stress increase followed by a plateau-region and densification, whereas VACNT foams show a gradual

increase of stress in time, until reaching densification. The presence of fibrous microstructure in the VACNT foams is responsible for the observed time-scale effects on the micro-scale deformation. In quasi-static or low-velocity impacts, the fibers form progressive buckles undergoing local stiffening followed by local instability. At higher-velocity impacts, the buckle formation does not have sufficient time to progress and it is replaced by progressive crushing. The fiber alignment and the diameter distribution also plays an important role in the stress–strain response where the low-density foams, with less aligned fibers show a pronounced linear regime that is followed by a prolonged plateau regime at moderate stress levels, whereas the high-density foams, with more aligned fibers show a nonlinearly, and gradually increasing stress without a significant stress-plateau.

In all cases, VACNT foams exhibit high resilience to impact by recovering more than 80% of the deformation upon unloading. The dynamic energy dissipation characteristics and the mechanical properties are highly controllable, for example by tailoring the foam's microstructure during synthesis varying hydrogen concentration in the carrier gas. We quantified the intrinsic density gradient of the VACNT foams to elucidate the observed fundamental deformation mechanisms. VACNT foams show superior mechanical properties, such as high modulus, compressive strength (peak stress), and energy dissipation characteristics, compared to similar foam-like materials. These properties suggest their use in lightweight materials for tunable vibration damping and energy absorbing applications.

4. Conclusions

In summary, we synthesized VACNT foams with bulk densities varying from 0.1 to 0.3 g cm^{-3} , utilizing different concentrations of hydrogen varying between 30% and 5% during the floating-catalyst CVD synthesis. We characterized their mass density and alignment using synchrotron X-ray scattering and mass attenuation and showed the existence of a density gradient along the foam's height, and the high alignment of CNT fibers. The bulk density and alignment are affected by the different hydrogen concentrations used for synthesis and lower concentration of hydrogen results in higher density and vertical alignment. We characterized the dynamic response of VACNT foams and showed that they exhibit complex rate-effects with a rate-independent loading response, and a rate-dependent unloading response up to a critical velocity of impact. They support shock formation when impacted at velocities higher than the critical velocity. We found that the critical velocity is a function of the foam's bulk density and increases with increasing density. We identified the fundamental deformation mechanisms using *in-situ* high-speed microscopy and *ex-situ* electron microscopy and showed that when the macroscale VACNT foams are compressed, VACNT bundles undergo collective sequential progressive buckling at microscale, and individual CNTs undergo bending and buckling, and exhibit wall wrinkling in the nanoscale. Such collective buckle formation and progression characterized by the local softening and stiffening in the stress–strain response is replaced by progressive crushing

when the sample undergoes shock compression. We correlated their fundamental deformation mechanisms and the resultant bulk mechanical properties to the measured foam microstructure, and demonstrated the effects of intrinsic density gradient and alignment of CNT fibers. VACNT foams exhibit superior properties compared to other foam materials with high elastic moduli, high compressive strengths and have exceptional energy absorption capabilities. Their highly controllable microstructure, lightweight and their ability to recover from extremely high deformations make them an attractive candidate for protective applications.

Acknowledgements

We thank Ludovica Lattanzi and Wei-Hsun Lin for assistance in preparing the educational video, Jan Rys (ETH Zurich) and Darwin Zwissler (UC Berkeley, USA) for assistance during experiments. We acknowledge financial support from the Institute for Collaborative Biotechnologies (ICB) under the contract W911NF-09-D-0001 with the Army Research Office (ARO). A portion of this work was performed under the auspices of the U.S. Department of Energy by Lawrence Livermore National Laboratory under Contract DE-AC52-07NA27344. X-ray characterization was performed at beamline 7.3.3 at the Advanced Light Source, which is supported by the Director, Office of Science, and Office of Basic Energy Sciences, of the U.S. Department of Energy under Contract No. DE-AC02-05CH11231.

Appendix A. Supplementary data

Three high-speed camera videos (educational egg-drop video, progressive buckling, shock formation), synchrotron X-ray scattering and mass attenuation measurement methods and results, definition of mechanical parameters and additional experimental data. Supplementary data associated with this article can be found, in the online version, at <http://dx.doi.org/10.1016/j.carbon.2014.12.006>.

REFERENCES

- [1] Tawfik S, De Volder M, Hart AJ. Structurally programmed capillary folding of carbon nanotube assemblies. *Langmuir* 2011;27:6389–94.
- [2] Aliev AE, Lima MD, Fang S, Baughman RH. Underwater sound generation using carbon nanotube projectors. *Nano Lett* 2010;10:2374–80.
- [3] Hata K, Futaba DN, Mizuno K, Namai T, Yumura M, Iijima S. Water-assisted highly efficient synthesis of impurity-free single-walled carbon nanotubes. *Science* 2004;306:1362–4.
- [4] Zhang M, Atkinson KR, Baughman RH. Multifunctional carbon nanotube yarns by downsizing an ancient technology. *Science* 2004;306:1358–61.
- [5] Zhang X, Li Q, Tu Y, Li Y, Coulter JY, Zheng L, et al. Strong carbon-nanotube fibers spun from long carbon-nanotube arrays. *Small* 2007;3:244–8.
- [6] Zhang M, Fang S, Zakhidov AA, Lee SB, Aliev AE, Williams CD, et al. Strong, transparent, multifunctional, carbon nanotube sheets. *Science* (80-) 2005;309:1215–9.
- [7] Das R, Liu B, Reynolds J, Rinzler A. Engineered macroporosity in single-wall carbon nanotube films. *Nano Lett* 2009.
- [8] Endo M, Muramatsu H, Hayashi T, Kim YA, Terrones M, Dresselhaus MS. Buckypaper from coaxial nanotubes. *Nature* 2005;433:476.
- [9] Lau KKS, Bico J, Teo KBK, Chhowalla M, Amaratunga GA, Milne WI, et al. Superhydrophobic carbon nanotube forests. *Nano Lett* 2003;3:1701–5.
- [10] Cao A, Dickrell PL, Sawyer WG, Ghasemi-Nejhad MN, Ajayan PM. Super-compressible foamlike carbon nanotube films. *Science* 2005;310:1307–10.
- [11] Gui X, Wei J, Wang K, Cao A, Zhu H, Jia Y, et al. Carbon nanotube sponges. *Adv Mater* 2010;22:617–21.
- [12] Misra A, Raney JR, De Nardo L, Craig AE, Daraio C. Synthesis and characterization of carbon nanotube-polymer multilayer structures. *ACS Nano* 2011;5:7713–21.
- [13] Pathak S, Lim EJ, Abadi PPSS, Graham S, Cola BA, Greer JR. Higher recovery and better energy dissipation at faster strain rates in carbon nanotube bundles: an in-situ study. *ACS Nano* 2012;6:2189–97.
- [14] Pathak S, Raney J, Daraio C. Effect of morphology on the strain recovery of vertically aligned carbon nanotube arrays: an in situ study. *Carbon NY* 2013;1:1–22.
- [15] Deck CP, Flowers J, McKee GSB, Vecchio K. Mechanical behavior of ultralong multiwalled carbon nanotube mats. *J Appl Phys* 2007;101:023512.
- [16] Suhr J, Victor P, Ci L, Sreekala S, Zhang X, Nalamasu O, et al. Fatigue resistance of aligned carbon nanotube arrays under cyclic compression. *Nat Nanotechnol* 2007;2:417–21.
- [17] Hutchens SB, Hall LJ, Greer JR. In situ mechanical testing reveals periodic buckle nucleation and propagation in carbon nanotube bundles. *Adv Funct Mater* 2010;20:2338–46.
- [18] Yaglioglu O. Carbon nanotube based electromechanical probes [MIT thesis]; 2007.
- [19] Raney J, Fraternali F, Daraio C. Rate-independent dissipation and loading direction effects in compressed carbon nanotube arrays. *Nanotechnology* 2013;24.
- [20] Qiu A, Fowler SP, Jiao J, Kiener D, Bahr DF. Time-dependent contact behavior between diamond and a CNT turf. *Nanotechnology* 2011;22:295702.
- [21] Teo EHT, Yung WKP, Chua DHC, Tay BK. A carbon nanomattress: a new nanosystem with intrinsic, tunable, damping properties. *Adv Mater* 2007;19:2941–5.
- [22] Xu M, Futaba DN, Yamada T, Yumura M, Hata K. Carbon nanotubes with temperature-invariant viscoelasticity from –196 degrees to 1000 degrees C. *Science* 2010;330:1364–8.
- [23] Yang X, He P, Gao H. Modeling frequency- and temperature-invariant dissipative behaviors of randomly entangled carbon nanotube networks under cyclic loading. *Nano Res* 2011;4:1191–8.
- [24] Daraio C, Nesterenko VF, Jin S. Highly nonlinear contact interaction and dynamic energy dissipation by forest of carbon nanotubes. *Appl Phys Lett* 2004;85:5724.
- [25] Misra A, Greer JR, Daraio C. Strain rate effects in the mechanical response of polymer-anchored carbon nanotube foams. *Adv Mater* 2009;21:334–8.
- [26] Raney JR, Misra A, Daraio C. Tailoring the microstructure and mechanical properties of arrays of aligned multiwall carbon nanotubes by utilizing different hydrogen concentrations during synthesis. *Carbon NY* 2011;49:3631–8.
- [27] Bedewy M, Meshot ER, Reinker MJ, Hart AJ. Population growth dynamics of carbon nanotubes. *ACS Nano* 2011;5:8974–89.
- [28] Meshot E, Hart A. Abrupt self-termination of vertically aligned carbon nanotube growth. *Appl Phys Lett* 2008;113107:90–3.
- [29] Futaba DN, Hata K, Yamada T, Hiraoka T, Hayamizu Y, Kakudate Y, et al. Shape-engineerable and highly densely

- packed single-walled carbon nanotubes and their application as super-capacitor electrodes. *Nat Mater* 2006;5:987–94.
- [30] Bedewy M, Meshot ER, Guo H, Verploegen EA, Lu W, Hart AJ. Collective mechanism for the evolution and self-termination of vertically aligned carbon nanotube growth. *J Phys Chem C* 2009;113:20576–82.
- [31] Thevamaran R, Daraio C. An experimental technique for the dynamic characterization of soft complex materials. *Exp Mech* 2014;54:1319–28.
- [32] Gibson L, Ashby M. *Cellular solids*. 2nd ed. Cambridge University Press; 1999.
- [33] Liu Y, Qian W, Zhang Q, Cao A, Li Z, Zhou W, et al. Hierarchical agglomerates of carbon nanotubes as high-pressure cushions. *Nano Lett* 2008;8:1323–7.
- [34] Worsley MA, Kucheyev SO, Satcher JH, Hamza AV, Baumann TF. Mechanically robust and electrically conductive carbon nanotube foams. *Appl Phys Lett* 2009;94:073115.
- [35] Pekala RW, Alviso CT, LeMay JD. Organic aerogels: microstructural dependence of mechanical properties in compression. *J Non Cryst Solids* 1990;125:67–75.
- [36] Woignier T, Reynes J, Hafidi Alaoui A, Beurroies I, Phalippou J. Different kinds of structure in aerogels: relationships with the mechanical properties. *J Non Cryst Solids* 1998;241:45–52.
- [37] Leventis N, Sotiriou-Leventis C, Zhang G, Rawashdeh A-MM. Nanoengineering strong silica aerogels. *Nano Lett* 2002;2:957–60.
- [38] Torrents A, Schaedler TA, Jacobsen AJ, Carter WB, Valdevit L. Characterization of nickel-based microlattice materials with structural hierarchy from the nanometer to the millimeter scale. *Acta Mater* 2012;60:3511–23.
- [39] Poncharal P, Wang Z, Ugarte D, de Heer WA. Electrostatic deflections and electromechanical resonances of carbon nanotubes. *Science* 1999;283:1513–6.
- [40] Barnes A, Ravi-Chandar K, Kyriakides S, Gaitanaros S. Dynamic crushing of aluminum foams: Part I – Experiments. *Int J Solids Struct* 2013:1–15.
- [41] Tan PJ, Reid SR, Harrigan JJ. On the dynamic mechanical properties of open-cell metal foams – a re-assessment of the “simple-shock theory”. *Int J Solids Struct* 2012;49:2744–53.